Microporous and Mesoporous Materials 240 (2017) 149–158

Contents lists available at ScienceDirect

Microporous and Mesoporous Materials

journal homepage: www.elsevier.com/locate/micromeso

Emulsion-mediated synthesis of hierarchical mesoporous-macroporous Al-Mg hydrotalcites

Davi D. Petrolini [a], Ernesto A. Urquieta-González [b], Sandra H. Pulcinelli [a], Celso V. Santilli [a], Leandro Martins [a, *]

[a] Instituto de Química, UNESP - Univ. Estadual Paulista, Rua Prof. Francisco Degni 55, CEP 14800-900, Araraquara, SP, Brazil
[b] Centro de Pesquisas em Materiais Avançados e Energia - Univ. Federal de São Carlos, Rodovia Washington Luis, km 235, CEP 13565-905, São Carlos, SP, Brazil

ARTICLE INFO

Article history:
Received 26 August 2016
Received in revised form
7 November 2016
Accepted 13 November 2016
Available online 15 November 2016

Keywords:
Hydrotalcites
Sol-gel synthesis
Paraffin-surfactant emulsion
Hierarchical porous structure

ABSTRACT

A new sol-gel method mediated by the use of paraffin emulsions is presented for the synthesis of hierarchical mesoporous-macroporous Al-Mg hydrotalcites. Prior to the synthesis, the construction of ternary diagrams for paraffin/surfactant/ethanol helped to identify the most suitable compositional synthesis domain. Two distinct regions, denoted L1 (transparent microemulsion) and L2 (opaque emulsion) were identified for low and high concentrations of paraffins, respectively. The ternary diagrams revealed some features: i) n-hexane (C6) had the smallest L2 region; ii) the high viscosity of n-octadecane (C18) did not allow control of phase separation, and iii) the most suitable paraffin for the use as the emulsifier was the intermediate-sized n-dodecane (C12). The use of paraffin in concentrations included in the L1 region did not contribute to the creation of pores, but the emulsion templating in the L2 region led to hierarchical porous hydrotalcites when were calcined up to 250 °C having enhanced textural properties and presenting mesopores and macropores with mean sizes of 0.02 and 1 μm, respectively. The slit-like shaped mesopores were caused by the partial exfoliation of hydrotalcite layers unordered packed around the emulsion droplets, while the macropores arose from voids left by the droplets after thermal treatment. The singular textural properties of the studied Al-Mg hierarchical porous hydrotalcites turns the emulsion mediated-synthesis a potential method to obtain more efficient catalysts to be used in process involving bulky molecules.

1. Introduction

As well known, hydrotalcites exhibit many valuable features that enable their use as supports, catalysts, or catalyst precursors [1,2]. These substances are lamellar hydroxides that have the common formula $[M^{2+}_{1-x}M^{3+}_{x}(OH)_2]^{x+}A^{z-}_{x/z}$, where M^{2+} stands for a divalent cation, M^{3+} for a trivalent cation, and A^{z-} for the charge compensating anion. Considering the usual Mg^{2+} and Al^{3+} hydrotalcites, changes in the relative contents of Al and Mg alter the chemical acid-base and textural properties of the material [1,3–9], with established pure and crystalline hydrotalcite structures having compositions in which the molar value of x ranges from around 0.2 to 0.55 [7,10]. The Al and Mg cations distribute themselves randomly into the layers of crystalline brucite-like structure [3,10–16]. At higher values of x, a greater quantity of Al^{3+} octahedrons leads to the intercalation of larger amounts of anions, and as a consequence, the high density of Al^{3+} leads to a mixture of low crystallinity oxides. As hydrotalcite-like materials have several applications as support or catalyst, the fine-tuning of their porous structure is highly desirable [17–23].

These materials are simple and inexpensive to synthesize using a mixture of di- and trivalent salts and aging of the solution until precipitation occurs. The co-precipitation is generally performed with Na_2CO_3 solutions [17–19]. Another method, which produces materials with diverse textural properties, involves precipitation of the metal cations in a solution containing urea or acetate anions [17,18,22,24]. Thermal decomposition of the organic precursors used in the synthesis leads to gaseous products that break through the stacked brucite layers and cause exfoliation, consequently creating a mesoporous structure [22,24]. Alternatively, the synthesis can be performed by a sol-gel transition method. The

* Corresponding author.
E-mail address: leandro@iq.unesp.br (L. Martins).

http://dx.doi.org/10.1016/j.micromeso.2016.11.011
1387-1811/

versatility of the sol-gel method lies in the possibility of the combined use of organic pore templates such as polymers, surfactants, and emulsions [20,21,25–28].

An important feature of the emulsion-mediated synthesis of materials is that in an oil-in-water (O/W) type emulsion, it is possible to use an aqueous dispersion of solids in combination with the sol-gel transition. The entrapment of the dispersed oil droplets by the continuous phase occurs during the sol-gel transition of the system, induced, for example, by a rise in pH [25,26]. Furthermore, the addition of a surfactant to the emulsion can not only control the sizes of the droplets [27–29], but also intermediate the kinetic stability of the emulsion due to its presence between the oil-water interfaces, avoiding agglomeration of the isolated droplets [25–29]. It is easy to see that the method offers a mean of tuning pores of a predetermined size range, controlled by the droplet size. After the removal of the oil droplets by firing, a material with a structured pores arrangement could be obtained.

Emulsion-mediated syntheses are considered by many authors as a great tool for structural control because it is easy to manufacture a wide range of pore sizes. Materials as porous silica, metal oxides, carbons, and metals have been templated with emulsions and demonstrate the flexibility of this technique to form solid porous materials. The system which has been most extensively studied involves a W/O emulsion containing styrene and divinylbenzene as the continuous phase [30–32].

The present work describes a new sol-gel emulsion-mediated methodology for the synthesis of Al-Mg hydrotalcites with hierarchical mesoporous and macroporous structure, varying the relative proportions of Al and Mg and the amount and chain size of the paraffin used as an emulsifier, with the aim of independently control the size and frequency of the mesoporous and macroporous arrangements of the produced hydrotalcites. The impact of that resulting porous structure in the textural properties in comparison with hydrotalcites conventionally prepared, it is also discussed.

2. Experimental

2.1. Synthesis of the hierarchical mesoporous and macroporous hydrotalcites

The synthesis of the hierarchical hydrotalcites involved the use of aluminum tri-sec-butoxide ($Al(i\text{-}But)_3$) and magnesium nitrate as sources of the hydrotalcite framework. The assembly of the emulsified system employed linear alkanes (n-C_6H_{14}, n-$C_{12}H_{26}$, or n-$C_{18}H_{38}$), the non-ionic block copolymer Pluronic P123 (20 EO: 70 PO: 20 EO, 5826.38 g/mol), and ethanol as solvent. Pluronic P123 and the linear alkanes are known organic pore structure directing agents (PSDAs). Water was not a suitable solvent because it caused high exothermic hydrolysis of the aluminum tri-sec-butoxide, resulting in fast separation of the hydrotalcite/emulsion phases.

The dispersion of the oily phase in ethanol was conducted at room temperature for n-C_6H_{14} and n-$C_{12}H_{26}$, and close to the melting point of 30 °C for n-$C_{18}H_{38}$. The final molar composition of the sol was: 0.01 Pluronic: x ($Al(O\text{-}i\text{-}But)_3$): 1-x $Mg(NO_3)_2$: 15 ethanol. The dropwise addition of a 29 wt% solution of ammonium hydroxide, under stirring, led to the sol-gel transition and definitive trapping of the paraffin droplets in the gel.

In a typical synthesis procedure, 3.05 g of the Pluronic P123 surfactant was dissolved in 3.62 g of ethanol at room temperature (using n-$C_{12}H_{26}$ paraffin), followed by addition of 0.65 g of aluminum tri-sec-butoxide. The emulsification occurred by addition of amounts of n-$C_{12}H_{26}$ varying from 30 to 80 wt%. This was the only paraffin used to obtain the porous hydrotalcites after obtaining the information provided by the ternary diagrams. Subsequently, after complete dissolution of the reactants and homogenization of the reaction mixture, the growth of hydrotalcite layers around the dispersed droplets was initiated by adding 0.67 g of magnesium nitrate. The flasks containing the reaction mixtures were covered with polyethylene film and kept under stirring for 5 h. Instantaneous gelation occurred by adjustment of the pH to 10 with a NH_4OH solution. The gel formed was dried under 100 mPa of vacuum, at room temperature, during 48 h. The as-synthesized hydrotalcite precursor gels were calcined for 2 h under a flow of air, using two temperature plateaus, the first at 220 °C (corresponding to the boiling point of n-$C_{12}H_{26}$) and the second at 500 °C. After calcination, the hydrotalcite structure collapsed, giving rise to mixed oxides of Al and Mg. The hydrotalcite structure was reconstructed due to the memory effect by exposing the calcined hydrotalcite under air atmosphere saturated with water vapor. The characterizations refer to the reconstructed hydrotalcite structure.

For the sake of comparison, hydrotalcite counterparts synthesized without any organic template were also used in this study. The nomenclature of the samples was according to the mole ratio of aluminum ($Mg^{2+}_{1-x}Al^{3+}_{x}$) and the weight percentage of paraffin, in the form Alx-Pwt.%. For example, Al0.5-P60 refers to the sample with a Al^{3+} molar ratio of 0.5 and 60 wt% of n-$C_{12}H_{26}$.

2.2. Characterization of the emulsions and hydrotalcites

The effect of n-$C_{12}H_{26}$ on the emulsion properties was investigated using measurements of the hydrodynamic size of the oil droplets and the ionic conductivity. The hydrodynamic size of the dispersed oil droplets was determined from quasi-elastic light scattering (QELS) measurements, employing a laser light source (25 mW) with a wavelength of 532 nm, a goniometer (Brookhaven BI200SM) with pinhole photodetector at 90° of the incident beam, and a photocorrelator (PCS100). The hydrodynamic diameter (d_h) was calculated from the measured diffusion constant (D) using the Stokes equation: $D = kT/3\pi\eta d_h$, where k, T, and η are the Boltzmann constant, the absolute temperature, and the solvent viscosity, respectively.

The electrical conductivity of the emulsion was measured at room temperature (≈25 °C) using a Marconi CA-150 conductimeter consisting of a conductivity cell fitted with Pt electrodes. Calibration of the conductimeter was performed using a 0.01 mol/L KCl solution.

The hydrotalcite porous structure was analyzed by skeletal (ρ_s) and bulk (ρ_b) density measurements, employing helium (AccuPycc 1330, Micromeritics) and dried-fluid (GeoPyc 1360, Micromeritics) pycnometry, respectively. The open porosity (ε_P) was calculated from these density values using the relationship $\varepsilon_P = (1 - \rho_s/\rho_b)$. The pore size distribution was determined by mercury intrusion porosimetry, using an AutoPore III instrument (Micromeritics). Degassing of the samples prior to analysis was performed under vacuum below 0.05 mPa. The pore diameter was calculated by means of the Washburn equation [33], using surface tension of 0.489 N/m and contact angle of 135°.

Nitrogen adsorption-desorption isotherms of the studied samples were obtained at −195 °C and P/P_0 ranging between 0.001 and 0.998, using an ASAP 2010 instrument (Micromeritics). Prior to the measurements, the samples were degassed at 200 °C for 12 h under a vacuum of 0.01 mPa, which ensured that the hydrotalcite structure was preserved. The specific surface area was calculated according to the BET equation and the pore size distribution was determined using the BJH method.

The samples were analyzed by conventional X-ray diffraction using a Siemens D5000 diffractometer with CuKα radiation selected by a curved graphite single crystal monochromator. The step size was 0.02° every 1 s in the 2θ range between 3° and 80°. Phase analysis was performed by the Rietveld profile method, using

GSAS-EXPGUI software [34,35]. The refinement enabled definition of the trigonal unit cell parameters of the hydrotalcites ($a = b \neq c$; $\alpha = \beta = 90°$, $\gamma = 120°$). The scale factors, zero shifts, and backgrounds of the peak profiles and the lattice parameters were refined using a sixth-degree Chebyshev polynomial. Pseudo-Voigt functions were employed for the peak profile refinements. Other parameters were not refined.

In order to follow the transition of the hydrotalcite layers into the low crystallinity Al-Mg oxide structure, due to interlayer water release and decarbonization, *in situ* X-ray powder diffraction (XRD) analysis was carried out during heating up to 500 °C, at a heating rate of 5 °C/min, under a flow of He, at the XPD beamline of the Brazilian Synchrotron Light laboratory (LNLS). The XPD beamline had a Huber 4 + 2 circle diffractometer equipped with an Eulerian cradle (Model 513), placed at ≈13 m from the double-bounce Si(111) monochromator (λ = 0.1377 nm) [36]. The data were collected in high-resolution mode employing a Si(111) analyzer crystal and a Mythen detector.

The hydrotalcites were observed by scanning electron micrographs (SEM), using a Philips XL 30 equipment. The samples were deposited on aluminum sample holder and sputtered with gold. Transmission electron microscopy (TEM) analyses were performed using a TECNAI G^2 F20 instrument operated at 200 kV. Samples were dispersed in methanol and left in an ultrasonic bath for 2 h, after which the suspension was dripped onto copper grids.

3. Results and discussion

3.1. Preliminary study of the formation of emulsion and its kinetic stability

A series of emulsions prepared using different mass ratios of Pluronic P123, paraffin, and ethanol were studied in order to determine the most suitable proportions for the synthesis of the hydrotalcites (Fig. 1 and Supplementary Material Fig. S1). As can be seen from Fig. 1, the transparent L1 region occurred at the extremes of the obtained diagrams, corresponding to paraffin-poor (<20%) and paraffin-rich (>80%) conditions. The area of the opaque L2 region increased according to increase of the hydrophobicity of the paraffins from C6 to C18 (Fig. S1). The emulsion with n-hexane showed the smallest L2 region. Although the experimental data indicated that the use of n-octadecane resulted in the greatest emulsified area, it was the hardest emulsion to handle due to its high viscosity.

The use of ethanol was necessary to ensure successful preparation of the porous hydrotalcites. However, it is known from the literature that short chain alcohols are detrimental to the kinetic stability of emulsions [37,38]. Therefore, in the first experiments, ternary phase diagrams were used to identify the stable region of the ethanol/paraffin/Pluronic emulsified system. The subsequent steps employed compositions corresponding to the regions of the ternary diagram in which the droplets of paraffin produced a stable and emulsified system.

The results shown in Fig. 2a, illustrating the evolution of the hydrodynamic size distribution of the paraffin droplets (indicated by the green arrow in Fig. 1a) and the specific conductivity (blue arrow), supported the visual interpretation of regions L1 and L2 as a function of the amount of n-dodecane. These experiments were performed using a constant mass proportion of Pluronic P123 and ethanol (50:50), similarly as used in the synthesis of the hydrotalcites. In region L1, with a low concentration of n-dodecane, there was the formation of a stable microemulsion, on the scale of 1–2 μm, which gave the characteristic transparency of this type of system (Fig. 1b). A narrow monomodal distribution of the hydrodynamic diameter was observed for emulsions containing less than 15 wt% of n-dodecane. However, a substantial broadening of the hydrodynamic diameter at 15 wt% indicated the presence of arbitrarily distributed larger interconnected domains caused by elongation of isolated droplets of n-dodecane. This corresponded to the transition between a microemulsion and an emulsion.

The hydrodynamic diameter measured in the concentrated L2 region were influenced to an extent by multiple scattering effects. However, the results confirmed the transition between the systems. Additionally, it is important to point out that the opaque appearance of the system, as well as its observed instability, are characteristic of emulsion formation. The ternary diagrams of Fig. 1a also show (open symbols) the data points for the emulsion-forming region with low kinetic stability (<3 min). Phase separation was favored in three situations: (1) conditions rich in paraffin and poor in the stabilizing Pluronic P123 surfactant (lower region of the diagram); (2) with the use of n-octadecane, due to its greater hydrophobicity; and (3) where the surfactant was absent (see Fig. S1).

Despite the poorer stability of the emulsion in the lower region of the diagram, these conditions were also considered in the synthesis. With rapid condensation of the hydrotalcite precursors, the viscosity of the emulsion increased, hence improving the kinetic stability of the emulsified system. Moreover, simultaneous stirring of the sol and adjustment of the pH to 10 resulted in formation of a tridimensional framework of gelled hydroxides of aluminum and magnesium, which permanently entrapped the paraffin droplets.

The compositional domains of the n-dodecane emulsion formation were also investigated using measurements of electrical conductivity, revealing the occurrence of two different regions, below and above 80 wt% n-dodecane (Fig. 2b). For concentrations <80%, the specific conductivity declined continuously, reflecting

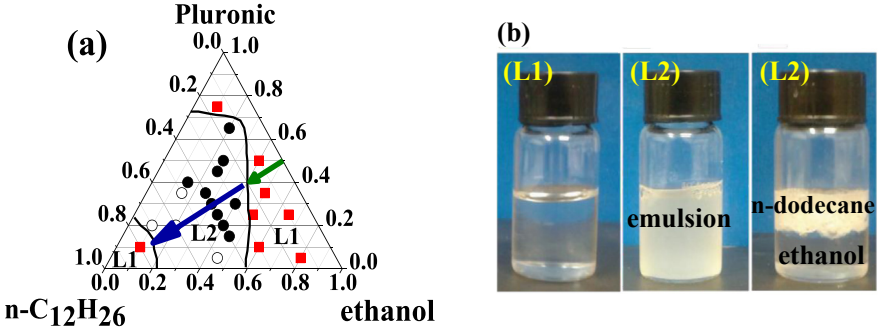

Fig. 1. (a) Emulsions of n-dodecane phase diagram. The microemulsion region is indicated by L1 (■), while the region L2 indicates the emulsion region. The filled black symbols indicate greater kinetic stability (● > 3 min) and the unfilled ones low stability (○ <3 min); (b) Images of the samples in the regions L1 and L2 (a few seconds after stirring), and in region L2 with flotation of n-dodecane due to phase separation after 3 min.

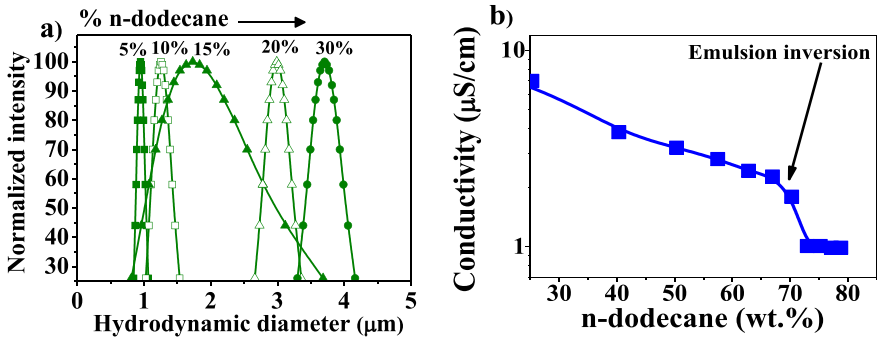

Fig. 2. (a) Evolution of the hydrodynamic diameter; (b) specific conductivity of the emulsion as a function of n-dodecane weight %, with the surfactant and ethanol contents being kept constant at 50% according to the isopleths indicated in Fig. 1(a).

the smaller amount of the continuous ethanol phase (which is more conducting than n-dodecane) in the emulsion. The extra amount of n-dodecane added at around 70 wt% caused a sharp decrease in the specific conductivity, indicating that the ethanol phase became discontinuous due to emulsion inversion.

Based on these initial experiments and the results obtained with the ternary diagrams, n-dodecane was adopted as the most suitable paraffin for preparation of the emulsions.

3.2. Effects of the quantity of paraffin and the molar fractions of aluminum and magnesium on the porous characteristics of the hydrotalcites

The sol-gel method combined with the n-dodecane emulsion produced a porous hydrotalcite (Figs. 3 and 4) that was free from phase impurities such as residual MgO or Al_2O_3. Fig. 5 shows the diffraction peaks of samples produced using a fixed amount of n-dodecane (Alx-P60), with the hydrotalcite structure consisting of layered mixed oxyhydroxides with brucite-like layers. The diffractograms shown in Fig. 5a correspond to samples calcined at 500 °C that underwent subsequent reconstruction after several days of exposure to air and water vapor. The use of *in situ* XRD to monitor the thermal decomposition of hydrotalcite sample Al0.5-P50 (Fig. S2) revealed changes in the microstructure, with an ordered layer transforming to a highly disordered, dehydrated, layered structure, and finally to a very low crystallinity Al-Mg

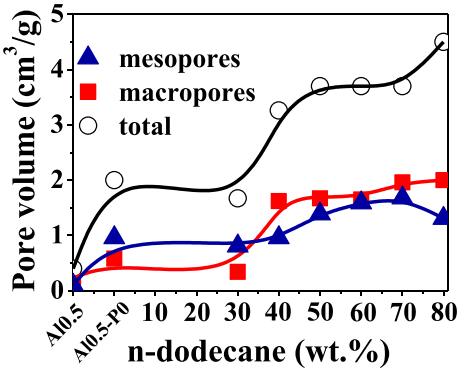

Fig. 4. Pore volumes of the hydrotalcites as a function of the weight percentage of n-dodecane.

mixed oxide with periclase structure. The X-ray diffractograms shown in Fig. 5a indicated the presence of a crystalline hydrotalcite for values of x = Al/(Al + Mg) between 0.2 and 0.6. Outside this compositional range, crystalline phases comprising mainly magnesium (x < 0.2) or aluminum (x > 0.6) oxides were also detected. The unit cell parameters "a" and "c" were calculated for the hydrotalcite structures with hexagonal 3R symmetry (where "a" is equal to "b"). The results (Table 1) showed that the value of "c"

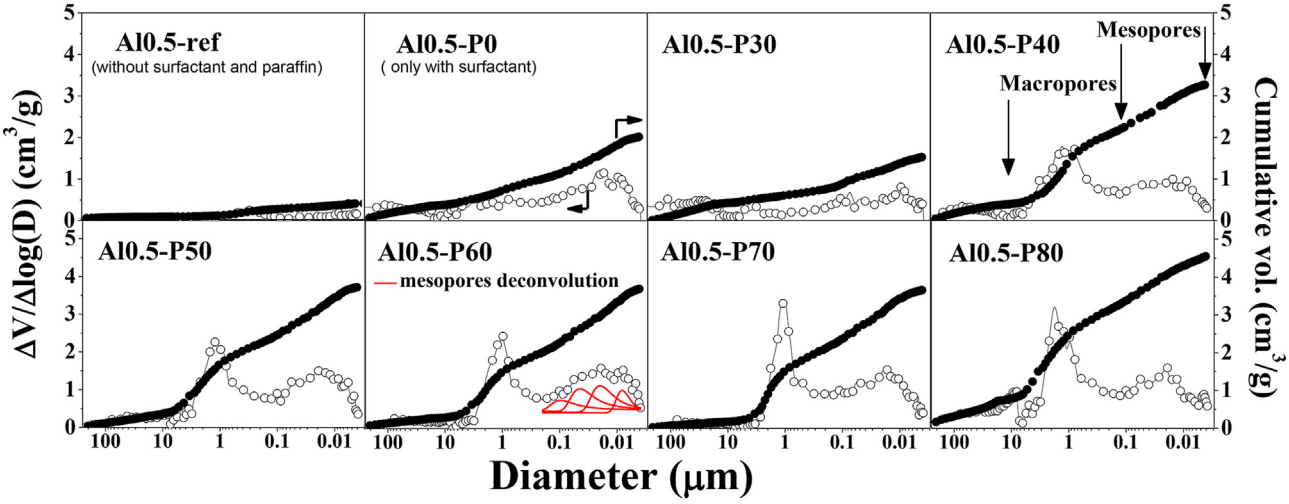

Fig. 3. Pore size distribution (open symbols) and cumulative pore volume (closed symbols) determined by mercury intrusion porosimetry of the hydrotalcite samples prepared with emulsions of n-dodecane. For sample Al0.5-P60, the broad mesopore distribution is deconvoluted into several families of mesopores of distinct sizes (in red).

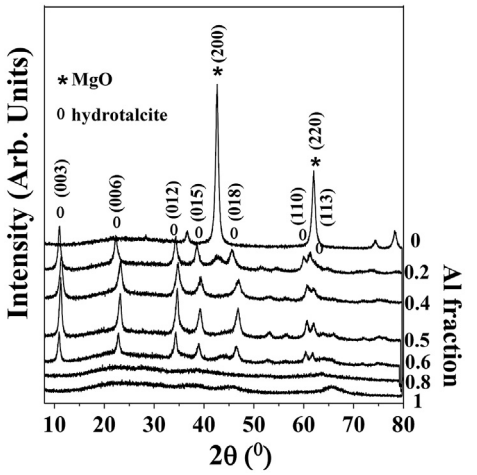

Fig. 5. X-ray diffractograms of the Alx-P60 samples synthesized using different aluminum molar fractions.

from the voids left after removal of the paraffin droplets by the thermal treatment. In the case of the mesopores, there are two possible source mechanisms. They could originate from the cylindrical micelles of the surfactant (as cylindrical pores) or from the mismatched packing of the hydrotalcite layers around droplets of the emulsion (as slit-like pores). As mentioned before, the main purpose of using the surfactant was not to provide a template for the generation of mesopores, but rather to modify the energy state at the interface in order to stabilize the emulsions, which would exhibit a strong tendency for flotation in the absence of a surfactant. If the quantity of surfactant in the mixture exceeded the quantity necessary to form monolayers at the ethanol-oil droplet interfaces, part of it could migrate to the continuous ethanol phase, forming micelles that could act as soft templates for mesopores.

In this study, the very small surfactant/ethanol molar ratio of 0.01/15 seemed unlikely to lead to saturation of the oil/ethanol interface. Therefore, the mesopores probably arose from the disordered packing of the hydrotalcite layers. The deconvolution of the mesopore peaks of sample Al0.5-P60 (highlighted in red in

Table 1
Specific surface areas and lattice parameters of the hydrotalcites synthesized in the absence and in the presence of the organic pore structure directing agents (PSDA = n-dodecane and surfactant). The measured ε_P porosities of selected samples are indicated in parentheses.

Samples without PSDA and different Al/(Al + Mg) ratios			Samples with different PSDA amounts and Al/(Al + Mg) = 0.5			Samples with different Al/(Al + Mg) ratios and 60 wt% of n-dodecane		
Sample	BET area (m^2/g) and ε_P (%)[a]	Lattice parameters a and c (nm)	Sample	BET area (m^2/g)	Lattice parameters a and c (nm)	Sample	BET area (m^2/g) and ε_P (%)	Lattice parameters a and c (nm)
Al0.0-ref	15 (57.6)	–	Al0.5-P0	119	0.3026; 2.2572	Al0.0-P60	29 (86.1)	–
Al0.2-ref	7	0.3076; 2.3946	Al0.5-P30	191	0.3029; 2.2599	Al0.2-P60	33	0.3076; 2.3733
Al0.4-ref	7	0.3045; 2.3202	Al0.5-P40	231	0.3032; 2.2634	Al0.4-P60	147	0.3036; 2.2790
Al0.5-ref	7 (70.2)	0.3034; 2.2648	Al0.5-P50	201	0.3035; 2.2656	Al0.5-P60	176 (75.4)	0.3033; 2.2624
Al0.6-ref	21	0.3031; 2.2598	Al0.5-P60	176	0.3033; 2.2624	Al0.6-P60	252	0.3030; 2.2606
Al0.8-ref	195	–	Al0.5-P70	162	0.3043; 2.2750	Al0.8-P60	416	–
Al1.0-ref	362 (75.4)	–	Al0.5-P80	262	0.3033; 2.2676	Al1.0-P60	468 (80.4)	–

[a] ε_P stands for porosity of the samples.

decreased gradually with increasing aluminum content, consistent with the isomorphic substitution of Mg-O (0.1963 nm bond length) by Al-O (0.1809 nm bond length) in the brucite-like structure. The changes could be monitored by the visual shift of the diffraction peaks. For the same fraction of aluminum, all the samples presented the same behavior in terms of the crystallographic parameter "c", independent of the presence of the PSDA in the synthesis mixture. Therefore, all the hydrotalcite structures had similar crystallographic fingerprints, based on the distribution of magnesium and aluminum atoms throughout the structure.

The ability of n-dodecane to generate pores in the solid hydrotalcites can be seen from the mercury intrusion porosimetry curves (Fig. 3) and the data in Table 1. Samples Al0.5-ref (without surfactant or n-dodecane) and Al0.5-P0 (with surfactant alone) were used to demonstrate the effect of addition of the emulsions. The presence of the surfactant in the gel led to total pore volumes from 0.5 to 1.9 cm^3/g, and finally to 3.1 cm^3/g in emulsified sample Al0.5-P40. Figs. 3 and 4 illustrate the origins of the two families of pores (macropores and mesopores) arising from the entrapment of the templates within the gelled structure. The typical meso- and macropore diameters remained centered at ≈0.02 and ≈ 1 μm, respectively, even when the n-dodecane content was increased from 30 to 80%. These results supported the conclusion that an increased percentage of oil led to a greater number of oil droplets in the emulsion.

From the emulsion-mediated synthesis of the porous hydrotalcites, it is reasonable to hope that the macropores are originated

Fig. 3) revealed the presence of several families of pores, as expected for slit-shaped voids formed from the irregular stacking of platelets. Fig. 4 shows the quantitative growth in the volumes of the mesopores and macropores, as a function of the n-dodecane percentage. The results summarized in Table 1 show that the addition of n-dodecane in the synthesis not only enhanced the porosity, but also increased the specific surface area. For example, between samples Al0.5-ref and Al0.5-P50, the porosity increased from 70.2 to 75.4%, while the specific surface area increased from 7 to 201 m^2/g.

The synthesis of the porous hydrotalcites also occurred in the presence of n-hexane and n-octadecane (Fig. S3). However, due to the features of the emulsions previously described, the porosities were somewhat inferior to those of the samples synthesized in the presence of n-dodecane. For example, in the case of sample Al0.5-P60 synthesized in the presence of n-hexane, n-dodecane, or n-octadecane, the total pore volumes were 1.5, 3.6, and 3.0 cm^3/g, respectively.

The mean mesopore and macropore sizes of the porous hydrotalcites were 0.02 and 1 μm. However, a remarkable change in the porous structures of the hydrotalcites was observed when the aluminum fraction was changed (Fig. 6). For samples Al0.6-P60 and Al0.8-P60, the macropores vanished completely, while at the same time the mesopore size distribution became thinner. Given the previous information based on the ternary diagram, which confirmed the formation of an emulsion using 60 wt% of n-dodecane, a possible explanation for the disappearance of

macropores is that there was a change in the way that the solid particles of Mg^{2+} and Al^{3+} in the sol were organized around the interface between the two phases. The XRD diffractograms (Fig. 5) showed that the lamellar hydrotalcite-like structure was no longer present. Additionally, the change in the composition of the Al-Mg species in the gel not only caused the hydrotalcite layers to vanish, but also led to the resulting adsorbed layer of solid particles forming a more rigid coating around the liquid droplets, resulting in compression of the droplets and a reduction in the size of the pores. Reorganization of surface materials around liquid droplets is predicted by the basic physico-chemistry of Pickering emulsions [39,40].

The changes in the pore structures of the hydrotalcites can also be seen in Fig. 7, with substantial decreases in macropore volume for aluminum fractions above 0.6. Based on these results, Fig. 8 shows an idealized representation of the arrangement of pores in the synthesized hierarchical porous hydrotalcites, with well-organized stacking of layers as well as random positioning around droplets. The scheme shows the macropore voids left by the droplets of n-dodecane, together with the slit-like arrangement of mesopores. Aiming to elucidate the regularity and ordering of the generated mesopores, small-angle X-ray diffraction (SAXRD) analyses were carried out and the results are shown in Fig. S4. As can be observed in the obtained diffractograms, no diffraction peaks were generated from the analyzed samples in that region, which indicated the inexistence of an ordered mesoporous structure in the studied solids.

Additional evidence concerning the mesoporous texture in the hydrotalcites was provided by the nitrogen physisorption

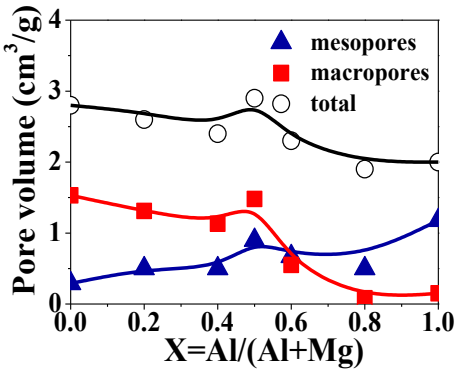

Fig. 7. Pore volumes of the hydrotalcites as a function of aluminum molar fraction.

experiments and the BJH pore size distribution curves obtained from the desorption branches of the isotherms (Fig. 9a). The hysteresis between the adsorption and desorption curves is typical of the existence of mesopores. However, the lack of a plateau in the P/P_0 region near 1 was characteristic of the type II isotherms often observed for solids in which macropores are also present. According to the IUPAC classification, the shallow slopes of the isotherms for the hydrotalcite samples, together with the non-parallel behavior of the adsorption and desorption curves, indicated a distinct H3 hysteresis loop. Moreover, for P/P_0 between 0.20 and 0.55, the mesopores distribution (Fig. 9b) was very broad, due to the different cross-sections of the slit-like pores. Finally, for P/P_0

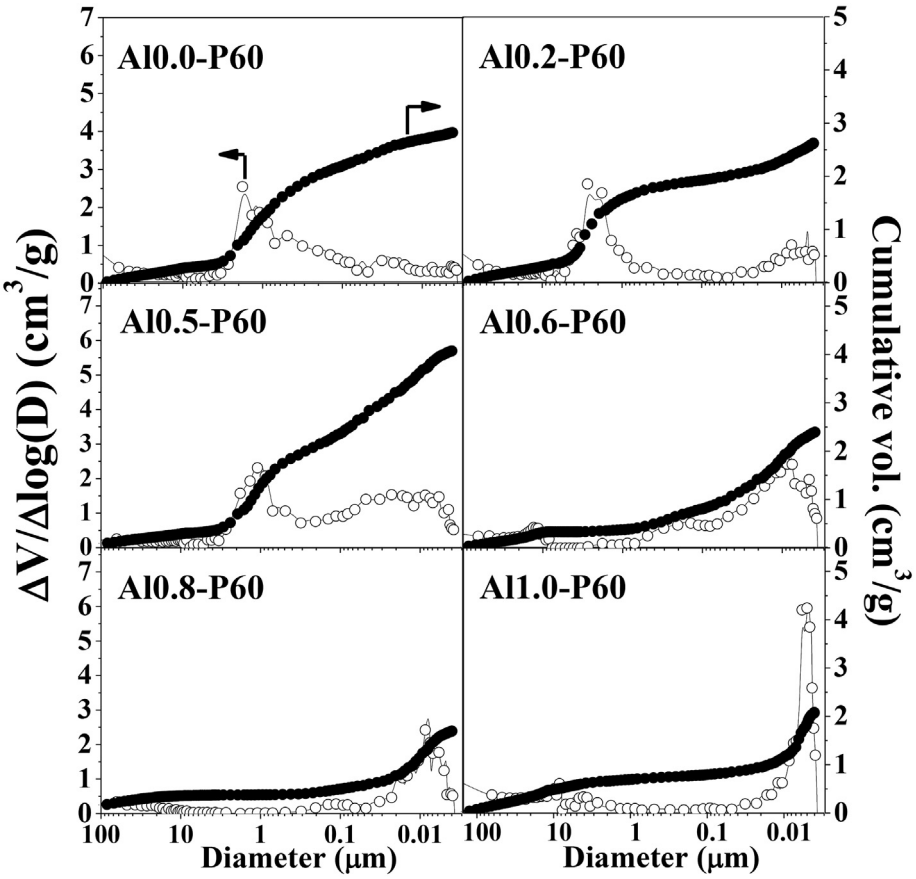

Fig. 6. Pore size distributions (open symbols) and cumulative pore volumes (closed symbols), determined by mercury intrusion porosimetry, for hydrotalcites prepared using different aluminum molar fractions.

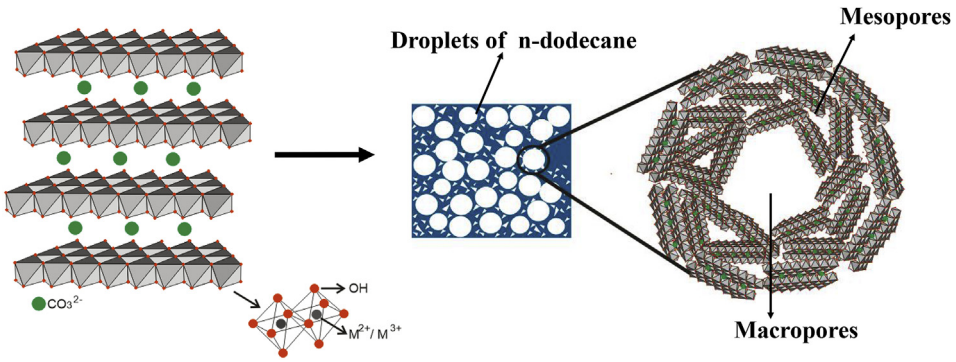

Fig. 8. Idealized representation of the pore arrangement resulting in a tactoid after emulsion-mediated synthesis of the porous hydrotalcites.

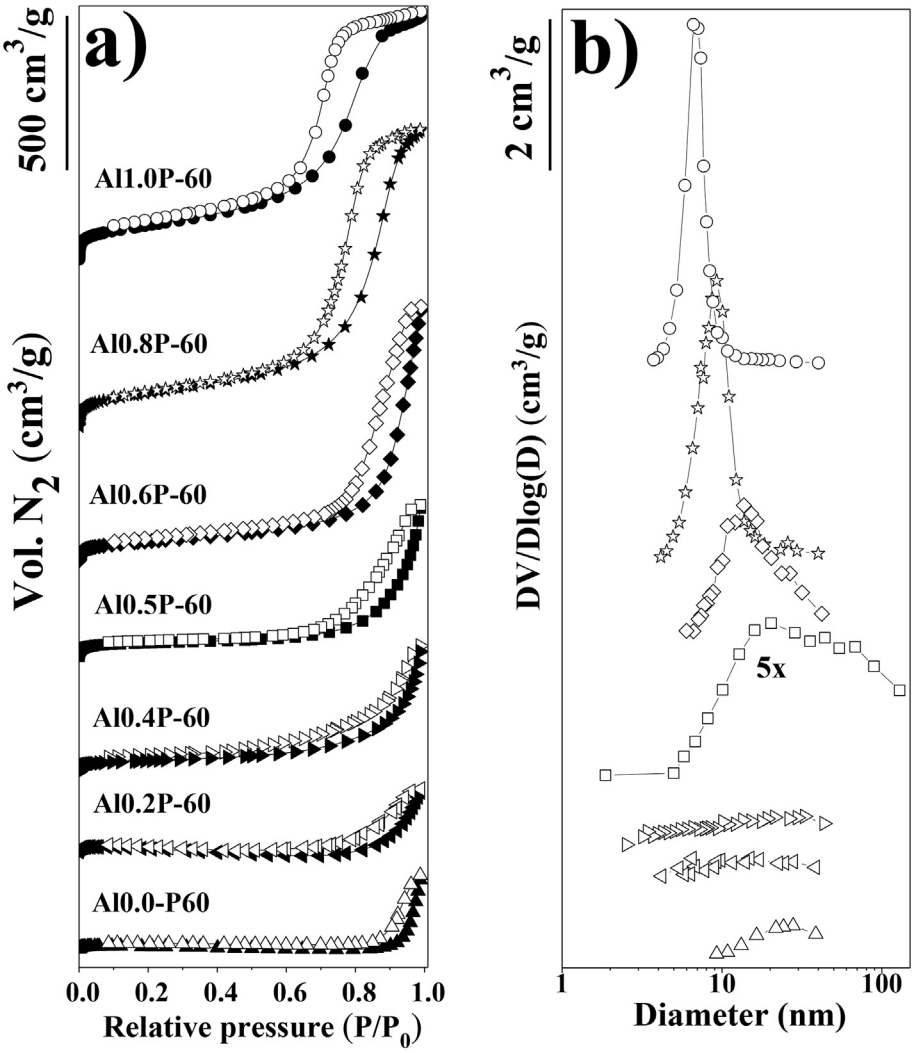

Fig. 9. (a) Nitrogen adsorption-desorption isotherms of the porous hydrotalcites with different molar fractions of aluminum; (b) BJH pore size distributions.

higher than 0.6, Fig. 9b shows an increase in narrow peaks below 10 nm (or 0.01 μm in the intrusion porosimetry measurements), which is the fingerprint for the formation of cylindrical pores.

An interesting aspect of these porous hydrotalcites is that they displayed a structural hierarchy, with lamellae at the finest level (according to the XRD data), while at the microscopic level there was the random packing of layers. In solids that exhibit such textural characteristic, these features are known as tactoids [37], composed of packets of parallel lamellae, such as platelets, together with sections of pores located in the inter-tactoid spaces. In this type of structure, an increase in the number of lamellae per tactoid acts to decrease the effective specific surface area. At another extreme, a ceramic composed of highly exfoliated lamellae would not show XRD patterns.

The transmission electron microscopy images and electron diffraction patterns of hydrotalcite samples are shown in Fig. 10. In fact, Al05-P60 sample had a random arrangement of the hydrotalcite layers confirmed by a diffraction pattern of concentric rings, due to the random orientation of small crystals of the polycrystalline material to produce a continuous angular distribution. On the other hand, the Al05-ref sample had a straight orientation of the particles and gave clear diffraction spots resulting from packed lamellae of hydrotalcite.

Scanning electron microscopy (SEM) images of the hydrotalcites (Fig. 11) provided evidence of the influence of n-dodecane on the texture of the samples. The reference hydrotalcite samples were initially composed of densely packed sheets. The microstructure and the surface topography were not appreciably different for Al0.2-ref and Al0.5-ref. For the Al0.8-ref sample (non-hydrotalcite structure), the near-smooth surface of the particle suggested an absence of pores. On the other hand, the samples prepared with addition of n-dodecane showed a granular structure, with coexistence of a smaller amount of cavities (resulting from the random stacking of small sheets) and voids between the granular particles. These altered morphologies were consistent with the expected change in the growth of the hydrotalcites associated with decreased aggregation growth under the effect of emulsification by addition of n-dodecane to the sol.

The use of surfactant and emulsion in the synthesis of these materials enabled generation of a novel arrangement of pores. In the case of the hydrotalcites, the use of surfactant and emulsion brought about a different type of stacking in the ethanol-n-dodecane interface, where the surface-facing OH groups of the hydrotalcites were not superimposed as expected for the interlayer region. The solid-liquid interface of the droplets substantially modified the tridimensional arrangement of the layers, as well as the layer-layer hydrogen bonding of the hydrotalcite layers at the interface. It is likely that the surface OH groups interacted with the hydrophilic parts of the surfactant molecules positioned at the interfaces of the droplets, forming local structures of hydrotalcite/surfactant/n-dodecane. The combination of results therefore suggests that the arrangement of pores illustrated in Fig. 8 was due to the stacking of successive layers that were set apart close to the emulsion-hydrotalcite interface. The well-ordered layers in the walls composed part of the hydrotalcite porous structure. This explanation is reasonable, considering the large sizes of the pores (1 μm) and the nanometric scale of the lattice parameters.

4. Conclusions

Novel Al-Mg mesoporous and macroporous hydrotalcites were obtained by a new one-step synthesis method based on the use of paraffin emulsions and surfactant as pore structure directing agents (PSDA), combined with sol-gel transition. The hydrotalcites produced in the emulsion-mediated synthesis presented well-defined hierarchical structures of mesoporous and macropores, exhibiting high specific surface areas and pore volumes, compared to their reference counterparts synthesized in the absence of the PSDA. Study of the emulsified paraffin/surfactant/ethanol system, together with information gathered from mercury intrusion porosimetry, led to the selection of n-dodecane for the production of suitable emulsions. Measurements of the electrical conductivity and quasi-elastic light scattering of the system consisting of n-dodecane/surfactant/ethanol indicated that n-dodecane contents in the range from 30 to 80 wt% were most suitable for the emulsion-mediated synthesis. These findings were subsequently confirmed using mercury intrusion porosimetry measurements and nitrogen physisorption isotherms for the synthesized hydrotalcites.

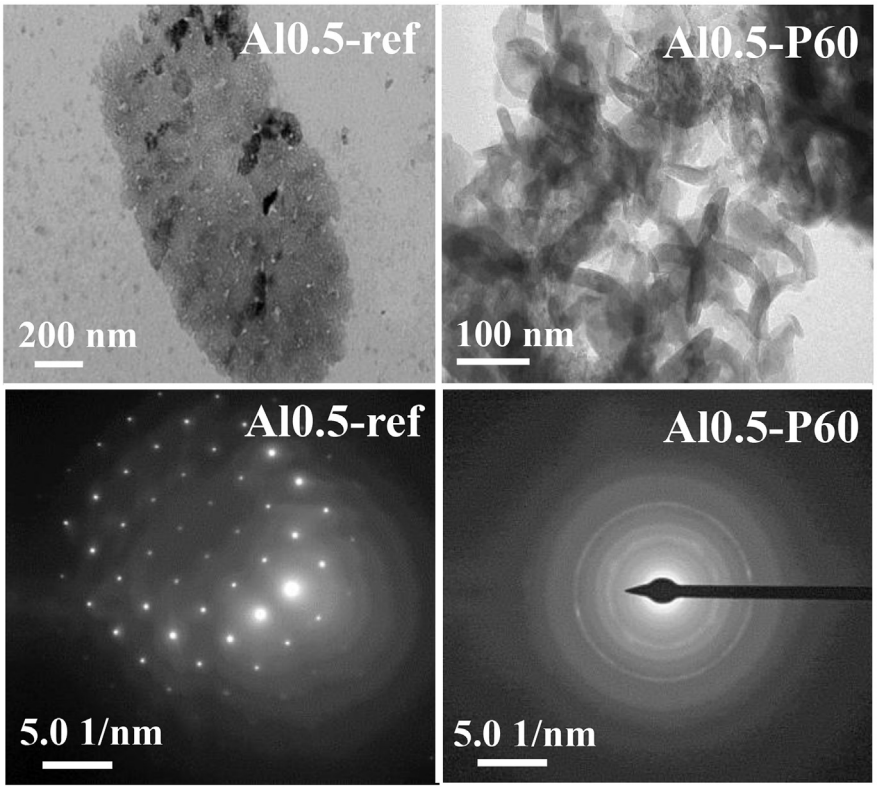

Fig. 10. Transmission electron microscopy images and electron diffraction of hydrotalcites Al0.5-ref and Al0.5-P60.

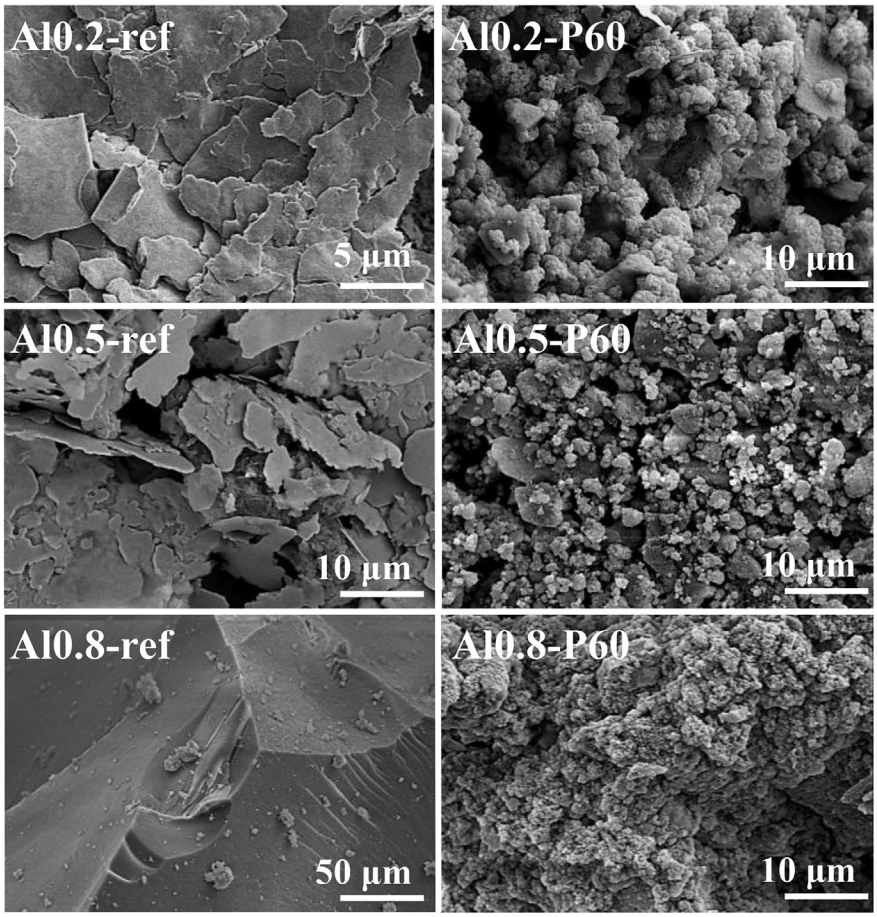

Fig. 11. Scanning electron microscopy images of hydrotalcites of aluminum and magnesium prepared in the absence or presence of 60 wt% n-dodecane.

The quantity of n-dodecane was effective for adjusting the creation of pores and for increasing the specific surface area of the material. Information provided by XRD confirmed a porous hydrotalcite-like material (for values of x = Al/(Al + Mg) between 0.2 and 0.6). The decrease of unit cell parameter "c" following increase in the aluminum fraction was the same for the emulsified and reference systems. The similar crystallographic fingerprints therefore showed that the templating process altered the bulk porosity, but did not affect the compositional microdomains. It could be concluded from the mercury intrusion porosimetry measurements and the nitrogen physisorption isotherms of the prepared porous hydrotalcites that the origin of the macropores was the entrapped paraffin droplets, while the slit-like mesopores were mainly derived from the spatial stacking of the layers organized around the droplets of paraffin.

Acknowledgements

This work was supported by the Brazilian agencies CNPq (grant 470094/2013-3) and FAPESP (grants 2013/01328-0 and 2015/05321-5). The authors also thank the Brazilian Synchrotron Light Laboratory (LNLS) in Campinas for use of the XPD beamline (proposal XPD-17839).

Appendix A. Supplementary data

Supplementary data related to this article can be found at http://dx.doi.org/10.1016/j.micromeso.2016.11.011.

References

[1] R. Jothiramalingam, M.K. Wang, Ind. Eng. 48 (2009) 6162.
[2] D. Tichit, C. Gerardin, R. Durand, B. Coq, Top. Catal. 39 (2006) 89.
[3] A. Corma, S. Iborra, J. Primo, F. Rey, Appl. Catal. A Gen. 114 (1994) 215.
[4] A. Corma, V. Fornés, F. Rey, J. Catal. 148 (1994) 205.
[5] V.K. Diez, C.R. Apesteguia, J.I. Di Cosimo, J. Catal. 215 (2003) 220.
[6] C.S. Castro, C. Ferreti, J.I. Di Cosimo, J.M. Assaf, Fuel 103 (2013) 632.
[7] J.I. Di Cosimo, G. Torres, C.R. Apesteguia, J. Catal. 208 (2002) 114.
[8] J. Bedia, J.M. Rosas, J. Marquez, J. Rodriguez-Mirasol, T. Cordero, Carbon 47 (2009) 286.
[9] M.M. Al-Daous, A.A. Manda, H. Hattori, J. Mol, Catal. A Chem. 363 (2012) 512.
[10] D.G. Cantrell, L.J. Gillie, A.F. Lee, K. Wilson, Appl. Catal. A Gen 287 (2005) 183.
[11] H. Morioka, Y. Shimizu, M. Sukenobu, K. Ito, E. Tanabe, T. Shishido, K. Takehira, Appl. Catal. A Gen. 215 (2001) 11.
[12] K. Akutu, H. Kabashima, T. Seki, H. Hattori, Appl. Catal. A Gen. 247 (2003) 65.
[13] A. de Roy, C. Forano, J.P. Besse, Layered Double Hydroxides: Present and Future, Nova Science Publishers, Huntington, 2001.
[14] Y.F. Gao, M. Nagai, Y. Masuda, F. Sato, W.S. Seo, K. Koumoto, Langmuir 22 (2006) 3521.
[15] S. Abelló, F. Medina, D. Tichit, J. Pérez-Ramírez, J.C. Groen, J.E. Sueiras, Y. Cesteros, Chem. Eur. J. 11 (2005) 728.
[16] Z.P. Xu, G.Q. Lu, Chem. Mater. 17 (2005) 1055.
[17] F. Malherbe, C. Forano, J.P. Besse, Microporous Mater 10 (1997) 67.
[18] J.C. Buffet, N. Wanna, T.A. Arnold, E.K. Gibson, P.P. Wells, Q. Wang, D. O'Hare, Chem. Mater. 27 (2015) 1495.
[19] G.G.C. Arizaga, K.G. Satyanarayana, F. Wypych, Solid State Ionics 178 (2007) 1143.
[20] Y. Dimitriev, Y. Ivanoa, R. Iordanova, J. Chem. Technol. Metall. 43 (2008) 181.
[21] S.P. Paredes, G. Fetter, P. Bosch, S. Bulbulian, J. Mater. Sci. 41 (2006) 3377.
[22] M.L. Occelli, J.P. Olivier, A. Auroux, M. Kalwei, H. Eckert, Chem. Mater. 15 (2003) 4231.
[23] Y. Yang, X. Zhao, Y. Zhu, F. Zhang, Chem. Mater. 24 (2011) 81.
[24] J.C. Roelofs, J.A. van Bokhoven, A.J. van Dillen, J.W. Geus, K.P. de Jong, Chem. Eur. J. 8 (2002) 5571.

[25] M.A.A. Rosa, E.P. Santos, C.V. Santilli, S.H. Pulcinelli, J. Non Cryst. Solids 354 (2008) 4786.
[26] L. Martins, D. Cardoso, P. Hammer, T. Garetto, S.H. Pulcinelli, C.V. Santilli, Appl. Catal. A Gen. 398 (2011) 59.
[27] A.R. Passos, L. Martins, S.H. Pulcinelli, C.V. Santilli, J. Sol Gel Sci. Technol. 63 (2012) 242.
[28] D.D. Petrolini, S.H. Pulcinelli, C.V. Santilli, L. Martins, J. Sol Gel Sci. Technol. 71 (2014) 9.
[29] Jeremie Nestor, et al., Facile synthesis of meso/macroporous dual materials with ordered mesopores using highly concentrated emulsions based on a cubic liquid crystal, Langmuir 29.1 (2012) 432.
[30] Haifei Zhang, Andrew I. Cooper, Synthesis and applications of emulsion-templated porous materials, Soft Matter 1.2 (2005) 107.
[31] Adam F. Gross, Andrew P. Nowak, Hierarchical carbon foams with independently tunable mesopore and macropore size distributions, Langmuir 26 (2010) 11378.
[32] T.G. Mason, J.N. Wilking, K. Meleson, C.B. Chang, S.M. Graves, Nanoemulsions: formation, structure, and physical properties, J. Phys. Condens. Matter 18.41 (2006) R635.
[33] E.W. Washburn, Proc. Natl. Acad. Sci. 7 (1921) 115.
[34] B.H. Toby, J. Appl. Crystallogr. 34 (2001) 210.
[35] A.F. Gualtieri, S. Ferrari, M. Leoni, G. Grathoff, R. Hugo, M. Shatnawi, S. Billinge, J. Appl. Crystallogr. 41 (2008) 402.
[36] H. Canova, A. Fontoura, R.T. Neuenschwander, B. Diaz, C.B. Rodella, J. Phys. Conf. Ser. 493 (2014) 012004.
[37] M.A.A. Rosa, L. Martins, S.H. Pulcinelli, C.V. Santilli, Soft Matter 9 (2013) 550.
[38] L. Martins, M.A.A. Rosa, S.H. Pulcinelli, C.V. Santilli, Microporous Mesoporous Mater. 132 (2010) 268.
[39] Y. Chevalier, M.A. Bolzinger, Colloids Surf. A 439 (2013) 23.
[40] C.J. Brinker, G.W. Scherer, Sol-gel Science: the Physics and Chemistry of Sol-gel Processing, Academic Press, 2013.